



# Characteristics of individual aerosol particles over Ürümqi Glacier No. 1 in eastern Tianshan, central Asia, China

Zhongqin Li<sup>a,b</sup>, Shuhui Zhao<sup>a,\*</sup>, Ross Edwards<sup>c,d</sup>, Wenbin Wang<sup>a</sup>, Ping Zhou<sup>a</sup>

<sup>a</sup> State Key Laboratory of Cryospheric Sciences/Tianshan Glaciological Station, Cold and Arid Regions Environmental and Engineering Research Institute, Chinese Academy of Sciences, Lanzhou 730000, China

<sup>b</sup> Northwest Normal University, Lanzhou 730030, China

<sup>c</sup> Desert Research Institute, Reno, NV 89512, USA

<sup>d</sup> Curtin University of Technology, Bentley WA 6102, Australia

## ARTICLE INFO

### Article history:

Received 3 June 2009

Received in revised form 15 March 2010

Accepted 2 September 2010

### Keywords:

Aerosol particles

Particle characteristics

SEM-EDX

Ürümqi Glacier No. 1

## ABSTRACT

Aerosol samples were collected during 2007 on the Ürümqi Glacier No. 1. Size, morphology, and elemental compositions of more than 38,000 particles were determined by scanning electron microscopy equipped with an energy dispersive spectrometer (SEM-EDX). Based on the morphology and elemental compositions, particles were classed into 5 groups: Si-rich particles; Ca-rich particles; Fe-rich particles; K-rich particles and S-rich particles. Most of the particles were irregular shaped mineral particles smaller than 2.5 µm (PM 2.5); only 1.7% of the particles (small Fe-rich particles and S-rich particles) may be emitted by anthropogenic activities, which suggested that natural processes are the primary source of PM 2.5. Backward air mass trajectory analysis suggests that the arid and semi-arid regions of central Asia are the primary source of PM 2.5 to the region.

© 2010 Elsevier B.V. All rights reserved.

## 1. Introduction

Aerosol particles are ubiquitous in the atmosphere and exert an important influence on global climate and the environment. They affect the Earth's radiation budget, and hence climate, directly through the scattering, and absorption of light and indirectly by acting as cloud condensation nuclei (Buseck and Pósfai, 1999). Increasing attention has been devoted to the study of aerosols; however, they still represent a major uncertainty in our knowledge of climate change due to high spatial and temporal variability in their atmospheric loading and properties. More detailed investigations on individual aerosol particles are necessary to predict their impact on regional/global climate change.

Preserving a history of climatic change and atmospheric composition, ice from alpine glaciers have been used to reconstruct paleo-climate and glaciochemical/particle records on a variety of time scales (Duan et al., 2007; Ming

et al., 2008). In order to interpret these records in terms of atmospheric composition the relationship between atmospheric composition and its transfer to glacier surfaces must be studied on a site to site basis (Sun et al., 1998; Zhao et al., 2006; Ming et al., 2007). Integral to these studies, the characterization of individual aerosol particles provides detailed information of aerosol particle size, morphology, chemistry and source.

Scanning electron microscopy combined with an energy dispersive spectrometer (SEM-EDX) is a powerful method for analyzing the properties of individual aerosol particles. It can provide specific information on particle size and morphology as well as elemental composition, surface coatings and agglomeration (Paoletti et al., 2002). It can also be used to investigate particle source (anthropogenic or natural) based on chemical composition and morphological characteristics (Bernabe et al. 2005). Recently, SEM-EDX has been used to study aerosols in urban areas to evaluate sources of atmospheric pollution (Yue et al., 2006; Slezakova et al., 2008; Srivastava et al. 2009). Few studies have investigated background aerosol conditions and anthropogenic impacts

\* Corresponding author. Tel.: +86 931 4967381; fax: +86 931 8275470.  
E-mail address: [shuhui.zhao@163.com](mailto:shuhui.zhao@163.com) (S. Zhao).

over remote areas or the complexity and heterogeneous nature of long-range transported aerosols (Reid et al., 2003; Leck and Bigg, 2008; Cong et al., 2010). While several studies (Hoornaert et al., 2004; Okada and Kai, 2004) have investigated central Asian dust sources, little is known with respect to individual aerosol particles over central Asian alpine glaciers, especially in the Tianshan Mountains.

The Tianshan Mountains (Tianshan), located at the center of the arid and semi-arid regions of central Asia, contains the most inland glaciers in the world. Dust storms (Asian dust) originating from the region are transported eastward, on a hemispheric scale, impacting eastern China, North and South Korea, Japan, and the United States. Transport and deposition of the dust plays a significant role in the biogeochemical cycles and atmospheric chemistry of the northern hemisphere (Arimoto et al., 2006). Glaciers over Tianshan provide a unique opportunity to improve our understanding of the long-range transport of dust aerosols in the mid- and upper-troposphere. A long-term study of aerosols and snowpack chemistry has been carried out (Sun et al., 1998; Zhao et al., 2006; Li et al., 2006, 2007) on Ürümqi Glacier No. 1 in the eastern Tianshan. However, most of these studies focused on soluble inorganic and organic ions through bulk analysis and provided no information regarding individual aerosol species. Yet the influence of aerosols on climate and the environment is highly dependent on the physical combination of individual chemical compounds and their mixing state as aerosol particles.

In order to understand the micro-properties of individual aerosol particles over a Tianshan glacier, aerosol samples were collected on the Ürümqi Glacier No. 1, in the eastern Tianshan, during 2007. The main purpose of this work was to determine the chemical and physical properties of individual aerosol particles using SEM-EDX.

## 2. Experiment

### 2.1. Site description

All samples used in this study were collected from Ürümqi Glacier No. 1 (43°06' N, 86°49' E), a valley glacier located at the headwaters of the Ürümqi River in the eastern Tianshan (Fig. 1), at the center of the Eurasian continent. The aerosol-sampling site was located in the percolation zone of the east branch at an altitude of 4130 m a.s.l. (Fig. 1). The glacier is composed of an east and west branch and currently occupies a total area of about 1.68 km<sup>2</sup>. While the glacier is retreating at its terminus, the glaciers equilibrium line has averaged an altitude of ~4050 m a.s.l. during the past forty years. Above the equilibrium line lie a superimposed ice zone and percolation zone, where the precipitation is ~700 mm yr<sup>-1</sup> (Li et al., 2003b). Precipitation primarily occurs from May to September and accounts for 90% of the annual precipitation. In the area surrounding the glacier evergreen vegetation exists between 1600 and 3400 m a.s.l. Regional atmospheric circulation is dominated by the westerly jet, which prevails high above the mountains. Mountain topography converts the westerly into cyclonic and anticyclonic circulations up to 4000 m. At the surface diurnal valley winds prevail from March through September (Zhang et al., 1994). In context of the region, the Tianshan are surrounded by vast desert areas: the Taklimakan Desert and the Qaidam basin desert to the south, Gurbantunggut Desert to the north, the Gobi Desert to the east, and Peski Muynikum and Peski Sary-Ishikotrau deserts to the west.

### 2.2. Sample collection

Thirty-eight total suspended particulate (TSP) samples were collected once a week in 2007. Aerosol samples were

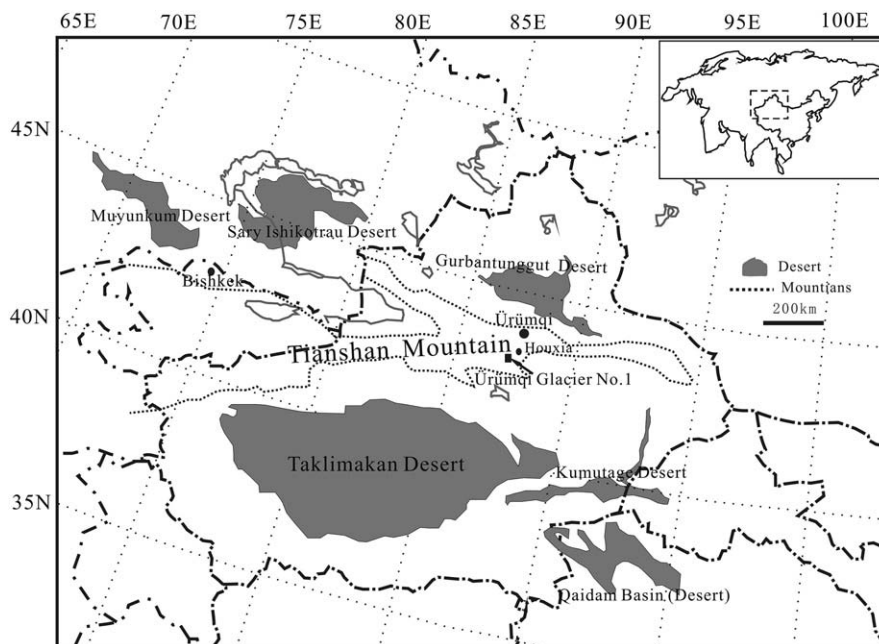


Fig. 1. Location map of Ürümqi Glacier No. 1 with geographic environment around the eastern Tianshan.

recovered on Zefluor™ Teflon filters (2.0 µm pore size, 47 mm diameter, Gelman Sciences) using a 12 V diaphragm pump powered by solar cells. Filters were loaded in the field and mounted face down about 1.5 m above the snow surface. The air volume through the filter was measured by an in-line meter and then converted into standard conditions according to the local ambient pressure and temperature. The particle collection efficiency (for particles as small as 0.035 µm) was estimated to be >97% based on the mean flow rate of 1.27 m<sup>3</sup>h<sup>-1</sup> over the filter (Liu et al., 1984).

The sampling period for each aerosol sample ranged from 3 to 9 h depending on weather conditions. No samples were collected during snow events. After sampling, filters were removed from the filter holder into cleaned airtight plastic containers and stored at 4 °C before analysis. When loading or unloading the filters, the operator wore plastic gloves and faced upwind in order to minimize contamination.

### 2.3. Sample analyses

Sections of the 47-mm diameter aerosol filters were cut off, mounted onto electron microprobe stubs, and coated with a thin gold film in order to get a higher quality secondary electron image. Individual particles were analyzed manually using a JEOL JSM-5600 LV scanning electron microscope (SEM) equipped with an energy-dispersive X-ray spectrometer (EDX/EDS). Operating conditions were: accelerating voltage = 20 kV; beam current = 60 µA; and spectral acquisition times = 30 s. SEM images were acquired at 1000, 2000, 5000, and 10,000 magnification. X-ray analysis was carried out with a conventional Si (Li) detector with a Be window capable of detecting elements with atomic numbers  $\geq 11$ . KeveX Quantex™ software for energy-dispersive microanalysis was used for the quantitative analysis of individual particles. The weight percent of elements was calculated based on characteristic X-rays. SEM pictures were further analyzed using Image-Pro Plus image processing and analysis software (Media Cybernetics, Inc. USA) as described by Yue et al. (2006) and Slezakova et al. (2008). Chose the manual measurement to target each of the particles on the image, the area and length were automatically measured by the software. The data were then exported into Microsoft Excel for further processing. Cluster analysis was used to identify different types of particles. More than 38,000 individual aerosol particles from 38 samples were examined using the SEM-EDX technique.

## 3. Results and discussion

### 3.1. Particle types classified by morphology and composition

Significant differences among the particles were found using SEM-EDX, indicating the diversity of aerosol types over the region. Examples of secondary electron micrographs and EDX diagrams for representative aerosol particles are shown in Fig. 2. To show the detected elements clearly, the EDX diagrams were redrawn from the original data without Au. Particle types were classified based on chemical composition and morphology. Similar to previous studies (Reid et al., 2003; Gao et al., 2007; Slezakova et al., 2008), cluster analysis was performed on particles from the 38 samples using the element composition determined by EDX, (Table 1). Cluster

composition was normalized by the relative weight of the elements analyzed, and the cluster number assigned arbitrarily. Defined clusters (C1–C18) represent at least 0.3% of the total number of particles examined. Grouping of clusters from all samples results in five major particle types.

#### 3.1.1. Silica-rich particles (abundance 55%)

Five clusters (C1, C5, C8, C9, and C17) with high Si are listed in Table 1. C9 represents a group of particles with Si relative abundance as high as 0.72 (Fig. 2a), suggesting the existence of mineral quartz (SiO<sub>2</sub>). C1, C5 and C17 are mainly comprised Si-Al-Ca, Si-Al-Fe-K and Si-Al-K, which may exist as aluminosilicates, such as feldspars, kaolinite, micas and smectite. Most particles in these clusters show irregular shapes (Fig. 2b), indicating terrigenous minerals sources. C8 has Si, Ca, Ti, K and Al as the main elements, and the ratio of Ca and Ti is about 1:1, which is likely to be from the aggregation of feldspars (or other aluminosilicate) and perovskite.

Si-rich particles identified as aluminosilicates/silica are the dominant particles in this area, which is similar to the results of aerosols collected from high Himalayas (Cong et al., 2010) and a remote station in Kazakhstan over Tianshan (Hoornaert et al., 2004). These particles can mainly be attributed to the surrounded dust sources or eolian dispersion of soil particles. A study at Qira in the Taklamakan Desert also found similar results with particles mainly composed of silicates (Okada and Kai, 2004).

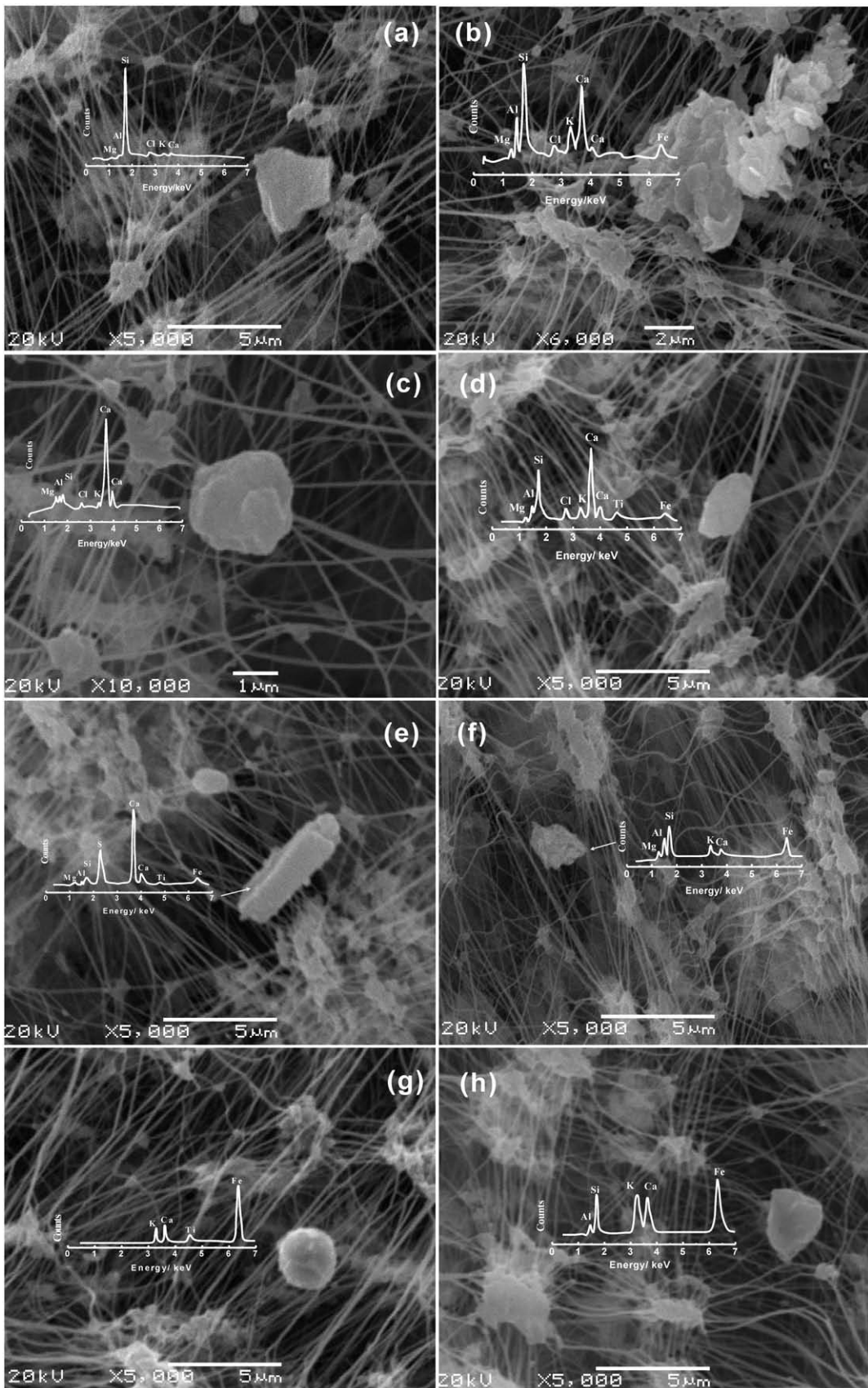
#### 3.1.2. Calcium-rich particles (abundance 30.1%)

C2, C4, C12, C15 and C18 are identified with a high abundance of Ca. Typical particles with irregular shapes are shown as Fig. 2c and d. C2 is probably CaCO<sub>3</sub> in the form of calcite. Previous studies of aerosol and snow soluble chemistry at the glacier found a predominance of Ca<sup>2+</sup>, HCO<sub>3</sub><sup>-</sup> and CO<sub>3</sub><sup>2-</sup> (Sun et al., 1998; Li et al., 2006), which also suggest the presence of CaCO<sub>3</sub>. C15 and C18 are associated with high Si, which may probably exist as micas, clay or CaCO<sub>3</sub> aggregated with other silicates. This is consistent with the findings of Okada and Kai (2004). Moreover, previous studies found that the region to the west of the Tianshan, between the Caspian and Aral Seas has the highest estimated amount of calcite on both a regional and global scale (Claquin et al., 1999). Aerosol particles collected from the desert and loess areas surrounding the Tianshan also contain a high mass proportion of Ca (Okada and Kai, 2004). Therefore these particles likely originate from local desert soils or through long-range transport from the west.

C12 is associated with high S, and perhaps existing as CaSO<sub>4</sub> aggregated with other species. It is probably natural gypsum or reaction products of carbonates with sulfuric acid. These particles also have irregular morphology (Fig. 2e), suggesting that calcium sulfates observed in this study are from terrestrial sources. While this cluster only accounts for ~1.4% of particles, it suggests that sulfate concentrations in snow or ice core from this area cannot be considered as a reliable proxy for anthropogenic pollution, special care should be taken to avoid misinterpretation.

#### 3.1.3. Fe-rich particles (abundance 6.5%)

C3, C11, C13, and C14 have a high abundance of Fe. C11 may exist as chlorite or other mineral particles with significant



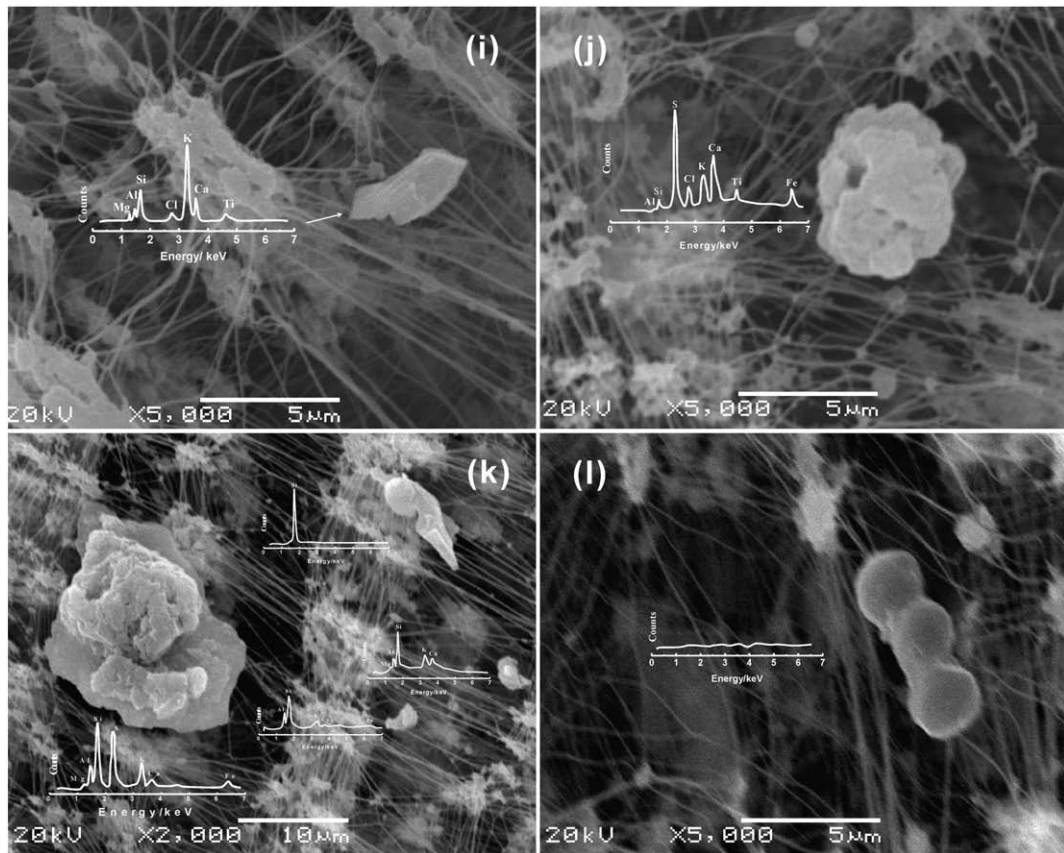


Fig. 2. Secondary electron images (SEI) of some aerosol particles on Ürümqi Glacier No. 1.

amounts of Fe, Si and Al, plus combinations of Mg, Cl, K, Ca and Ti. Because of the irregular morphology shown in Fig. 2f, these particles may originate from a natural source. Previous

research has shown that local exposed bedrock and glacial sediments are enriched in hydromica and chlorite containing Fe and Al (Luo, 1983). C13 represents a group of particles with

Table 1  
Individual-particle types determined by clustering and their relative abundance.

| Cluster | Type    | Cluster number | Number concentration (%) | Relative weight fraction |       |       |             |       |             |             |       |             |             |
|---------|---------|----------------|--------------------------|--------------------------|-------|-------|-------------|-------|-------------|-------------|-------|-------------|-------------|
|         |         |                |                          | Na                       | Mg    | Al    | Si          | Cl    | K           | Ca          | Ti    | Fe          | S           |
| A       | Si-rich | C1             | 12.6                     | 0.001                    | 0.01  | 0.12  | <b>0.51</b> | 0.071 | 0.092       | 0.12        | 0.054 | 0.016       | –           |
|         |         | C5             | 16.3                     | 0.001                    | 0.035 | 0.14  | <b>0.37</b> | 0.042 | 0.11        | 0.095       | 0.048 | 0.16        | –           |
|         |         | C8             | 3.1                      | –                        | 0.039 | 0.122 | <b>0.22</b> | 0.047 | 0.15        | 0.21        | 0.21  | –           | –           |
|         |         | C9             | 8.1                      | –                        | 0.01  | 0.061 | <b>0.72</b> | 0.043 | 0.068       | 0.058       | 0.029 | 0.011       | –           |
|         |         | C17            | 14.9                     | 0.001                    | 0.015 | 0.16  | <b>0.39</b> | 0.053 | 0.21        | 0.086       | 0.053 | 0.04        | –           |
| B       | Ca-rich | C2             | 7.3                      | –                        | 0.019 | 0.047 | 0.079       | 0.025 | 0.025       | <b>0.76</b> | 0.04  | 0.003       | –           |
|         |         | C4             | 0.6                      | –                        | –     | –     | –           | –     | 0.018       | <b>0.64</b> | 0.084 | 0.26        | –           |
|         |         | C12            | 1.4                      | –                        | 0.017 | 0.027 | 0.054       | 0.037 | 0.031       | <b>0.46</b> | 0.036 | 0.022       | 0.31        |
|         |         | C15            | 8.7                      | 0.001                    | 0.019 | 0.106 | 0.30        | 0.046 | 0.089       | <b>0.33</b> | 0.047 | 0.071       | –           |
| C       | Fe-rich | C18            | 12.1                     | 0.001                    | 0.039 | 0.078 | 0.16        | 0.046 | 0.062       | <b>0.53</b> | 0.063 | 0.025       | –           |
|         |         | C3             | 0.3                      | –                        | –     | –     | 0.13        | –     | 0.21        | 0.23        | –     | <b>0.44</b> | –           |
|         |         | C11            | 4.2                      | –                        | 0.045 | 0.15  | 0.30        | 0.036 | 0.073       | 0.041       | 0.032 | <b>0.33</b> | –           |
|         |         | C13            | 0.6                      | –                        | –     | –     | –           | –     | 0.027       | 0.096       | 0.051 | <b>0.83</b> | –           |
| D       | K-rich  | C14            | 1.4                      | –                        | –     | –     | –           | –     | 0.07        | 0.27        | 0.101 | <b>0.56</b> | –           |
|         |         | C6             | 7.0                      | 0.011                    | 0.017 | 0.102 | 0.18        | 0.16  | <b>0.20</b> | 0.17        | 0.102 | 0.01        | –           |
|         |         | C16            | 0.3                      | –                        | 0.015 | 0.078 | 0.09        | 0.069 | <b>0.56</b> | 0.11        | 0.075 | –           | –           |
| E       | S-rich  | C7             | 0.8                      | 0.016                    | 0.008 | 0.032 | 0.27        | 0.081 | 0.104       | 0.088       | 0.009 | 0.029       | <b>0.37</b> |
|         |         | C10            | 0.3                      | –                        | –     | –     | –           | –     | 0.082       | 0.19        | 0.11  | 0.14        | <b>0.48</b> |

Note: (a) The order of the elements in relative weight follows the order of the peaks appeared in the EDX spectrum except S; (b) cluster number assignment is arbitrary; (c) the most enriched element highlighted in bold; (d)– means that the relative weight fraction below 0.001 or not detected.

a relative Fe abundance as high as 0.83, which is indicative of Fe-Oxide. Besides soil dispersions, Fe-rich particles can also be emitted by coal-fired boilers, the metal industry, and power plants. Emitted by high-temperature furnaces, these particles are usually spherical (Cong et al., 2010). The spherical shaped particle from C13, shown in Fig. 2g, is therefore likely to have been emitted by a high temperature process. C3 and C14 are also abundant with Fe, but very different to C13 in their elemental composition and morphology. C3 and C14 have a higher abundance of Si, Ca and Ti than C13 and an irregular (nonspherical) morphology (Fig. 2h); the elemental composition suggests aggregates of Fe oxide, calcite and silicates. As apposed to C13, C3 and C4 are likely of natural origin.

### 3.1.4. K-rich particles (abundance 7.3%)

C6 and C16 have a high K content; Fig. 2i shows the morphology of one typical particle from C16. K is usually identified as a good tracer of biomass-burning aerosols (Li et al., 2003a). However, most biomass burning K rich particles have amorphous organic coatings or form small inclusions in organic particles (Li et al., 2003a). In our study, all the C6 and C16 particles had irregular shapes with no obvious amorphous coatings. According to their morphology and elemental composition, C6 and C16 are probably crustal in origin and aluminosilicates with high K content, such as feldspars and so on.

### 3.1.5. Sulfur-rich particles (abundance 1.1%)

C7 and C10 have sulfur as the major constituent element. These particles may be reaction products of  $\text{SO}_x$  and mineral dust particles. The particles were typically compact aggregates with hollow centers (Fig. 2j). Fossil fuel combustion, emits  $\text{SO}_x$  to the air, which can be absorbed onto the surface of the aerosol particles. In general mineral dust particles can act as a carrier for pollution species, such as trace gases and oxidants (Gao et al., 2007), which are absorbed onto the surface or react with it modify the physical structure of the particle. A large clay particle with a loosely held mass (Fig. 2k) is typical of this type and is usually associated with anthropogenic pollution.

Except for the five major groups, a few particles with undetectable elemental compositions were found (Fig. 2l). According to their morphology and other studies (Hu et al., 2009), they were likely organic particles or biological particles.

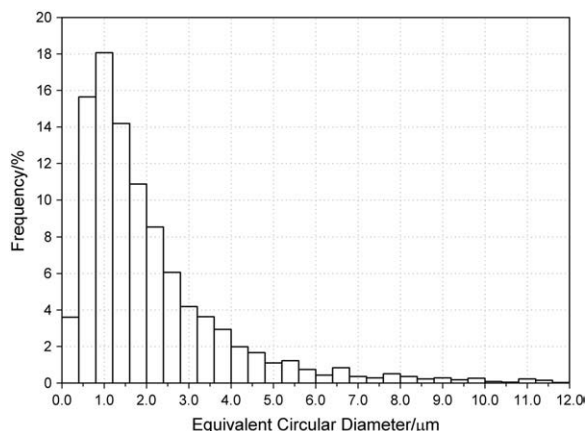


Fig. 3. Number-size distribution of the aerosol particles collected during 2007.

Further analysis of these particles was not performed because of their low occurrence. Moreover, soot particles, which originate from incomplete-combustions were rarely found in our samples, although they have been shown to be abundant in the aerosol particles collected over Ürümqi (Li et al., 2005). One possibility for this discrepancy is that the soot aerosol particles were small enough to pass through the filters.

In summary, ~98.3% of the detected particles over this region are probably from natural mineral dust. Only 1.7% (0.6% Fe-rich particles and 1.1% S-rich particles) of the particles may be have emitted by anthropogenic activities, suggesting that during the study period the site was not significantly impacted by anthropogenic pollution. Much attention has been focused on the impact of anthropogenic particles on the glacier as it has shrunk due to recent climate change. However, a previous study (Takeuchi and Li, 2008) revealed that dust particles on the glacial surface can reduce the glaciers surface albedo, accelerating its melt rate, and retreat. Consequently, the impact of mineral dust particles on the glacier's mass balance should not be ignored.

### 3.2. Particle size distribution

The particle number-size distribution can give insight into the variability of atmospheric transport and deposition processes, and provide information limiting possible sources. Direct physical particle sizes can be determined with electron beam microscopy (Scanning/Transmission Electron Microscope), and then equivalent particle sizes can be obtained from the microscope images. Several particle size definitions are in common use including: the mean of particles longest dimension and the orthogonal width (Okada and Kai, 2004; Hu et al., 2009); the square root of the particle area (Gao et al., 2007); and the diameter of a circle/sphere having equivalent area/volume, i.e. the equivalent circular diameter (ECD or average diameter)/equivalent spherical diameter (ESD) (e.g. Reid et al., 2003; Shi et al., 2003; Yue et al., 2006). In this study we used ECD (Eq. 1),

$$\text{ECD} = 2 \times \sqrt{\text{area}/\pi} \quad (1)$$

as an estimate of particle size. Ultrafine particles (ECD < 100 nm) passed through the filters resulting incomplete collection. Moreover, the images of ultrafine particles were so small that the calculated areas were highly uncertain. We therefore defined the lower ECD cutoff as 100 nm and excluded all particles < 100 nm.

The number-size distribution of individual particles > 100 nm are shown in Fig. 3. The particles primarily ranged from 0.1 to 10 μm with particles smaller than 2.5 μm (PM<sub>2.5</sub>) accounting for about 75% of the total number of particles. Seasonal variations of the number-size distributions are shown in Table 2. Variations in the distributions were found to coincide with seasonal variability in the total particle number (> 100 nm).

The annual maximum in total particle counts occurred in the boreal spring, coinciding with seasonal dust storm activity. The spring dust size distribution peak occurred from 1.0 to 2.5 μm, similar to the size distributions of mineral particles sampled in Beijing during Asian dust storm events (Shi et al., 2003). Minimum particle concentrations were found during the boreal winter indicating cleaner air

**Table 2**  
Seasonal variation of particle numbers, size distribution and precipitation.

| Seasons          | Particle number concentrations/% | Particle sizes distribution/% |                       |                       |                        |                     | Precipitation/mm |
|------------------|----------------------------------|-------------------------------|-----------------------|-----------------------|------------------------|---------------------|------------------|
|                  |                                  | <1.0 $\mu\text{m}$            | 1.0–2.5 $\mu\text{m}$ | 2.5–5.0 $\mu\text{m}$ | 5.0–10.0 $\mu\text{m}$ | >10.0 $\mu\text{m}$ |                  |
| Spring (Mar–May) | 41.0                             | 15.3                          | 52.7                  | 23.8                  | 7.1                    | 1.1                 | 114.5            |
| Summer (Jun–Aug) | 14.2                             | 37.3                          | 34.9                  | 17.5                  | 6.9                    | 3.4                 | 405.0            |
| Autumn (Sep–Nov) | 35.4                             | 41.8                          | 44.5                  | 10.2                  | 3.3                    | 0.2                 | 75.1             |
| Winter (Dec–Feb) | 9.4                              | 24.9                          | 42.1                  | 20.1                  | 9.7                    | 3.2                 | 9.2              |

conditions. The impact of pollution from the city of Ürümqi (population of 2,506,800, 105 km to the north east) on the glacier, has been debated over the past several years. In this study, no obvious impact was found, even in winter when particles <10  $\mu\text{m}$  ( $\text{PM}_{10}$ ) in Ürümqi are at their maximum. Low particle concentrations in winter may be attributed to the strong inversion layer between 1000 and 2400 m (Zhang et al., 1994). This inversion layer prevents air pollution diffusing to higher altitudes (Bi et al., 2007). Low particle concentrations during summer appear to be related to wet scavenging of particles by precipitation (Zhao et al., 2008). Because coarse particles are efficiently removed from the atmosphere by wet precipitation, particles in summer are very fine with ECDs smaller than 1.0  $\mu\text{m}$  and fall into the range of 1.0–2.5  $\mu\text{m}$ . Particles collected during autumn are distinct with the second largest number concentrations, and a higher proportion of particles smaller than 1.0  $\mu\text{m}$  than other seasons. Previous studies revealed that dust storms during May to September usually originate in central Asian regions such as Kyrgyzstan, Turkmenistan, Kazakhstan (Orlovsky et al., 2005; Semenov et al., 2005; Wu et al., 2008). We hypothesize that the autumn dust resulted from long-range transport of dust from these regions.

### 3.3. Particle shapes indicated by particle circularity

The particle shape is usually inferred by means of the roundness factor or circularity. In this paper, the circularity described by Gao et al. (2007) was used as follows:

$$C = L^2(4\pi A)^{-1}$$

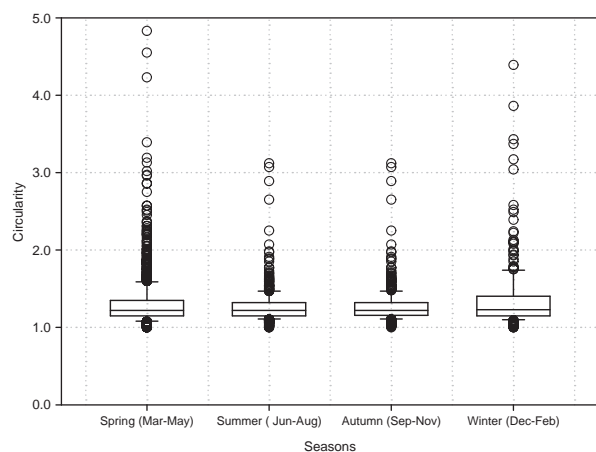


**Fig. 4.** Seasonal variations of particle shapes indicated by the degree of circularity.

Where  $C$  is circularity (non-dimensional),  $L$  is particle perimeter ( $\mu\text{m}$ ), and  $A$  is two-dimensional area of the particle in the SEM image ( $\mu\text{m}^2$ ).

Fig. 4 shows the seasonal variation of circularity distributions of individual particles in this area. Despite the possible bias toward lower circularity caused by the calculation problem discussed above, most of the particles have the circularity values more than 1.0. The circularity of the total particles examined ranged from 1.0 up to 6.1 (although the maximum value does not show up in the percentile plot), and most of the particles were more than 1.0, suggesting the non-spherical and complexity nature of the aerosol particles in this region. The median values of the particles in spring, summer, autumn and winter were 1.22, 1.21, 1.21 and 1.23 respectively. The degrees of shape complexity in the four seasons were almost the same, indicating minor shape variations between the different seasons. However, the 25th, 75th and 90th percentiles exist at different values during the four seasons, suggesting the difference distribution between them. The tendency of summer and autumn are almost the same, while spring and winter are similar. Circularity in spring and winter show a little bigger, indicating the particles are more complex.

Seasonal variations in circularity were similar to that of particle size. To explore whether a relationship existed between them, cumulative probability plots of circularity as a function of particle diameter were calculated (Fig. 5). The results show that circularity is dependent on size. Smaller particles have circularities near 1.0 while the largest particles have a median circularity of more than 1.5. This trend was also found in Asian dust by Okada et al. (2001), and is cited as evidence of increased particle complexity. With increased particle size, there is a higher probability that the particles are aggregates, and hence have a substantial increase in perimeter relative to area. This is compounded by the possibility of aggregates flattening on impact with the substrate (Reid et al., 2003). As a result the particle circularities in summer and autumn were smaller than in spring and winter.

### 3.4. Possible source regions of aerosols at Ürümqi Glacier No. 1

To identify potential transport pathways and possible source regions of aerosol at Ürümqi Glacier No. 1, air mass back-trajectories were calculated by the Hybrid Single-Particle Lagrangian Integrated Trajectory (HYSPPLIT) model of the Air Resources Laboratory of NOAA (Draxler and Rolph, 2003). HYSPPLIT back-trajectories have been used in previous studies (e.g., Marenco et al., 2006; Ming et al., 2008).

In this paper, mean trajectories ending at the sampling site during 2007 were simulated by the HYSPPLIT 4.8 model, as described by Ming et al. (2008). 5-day backward air trajectories

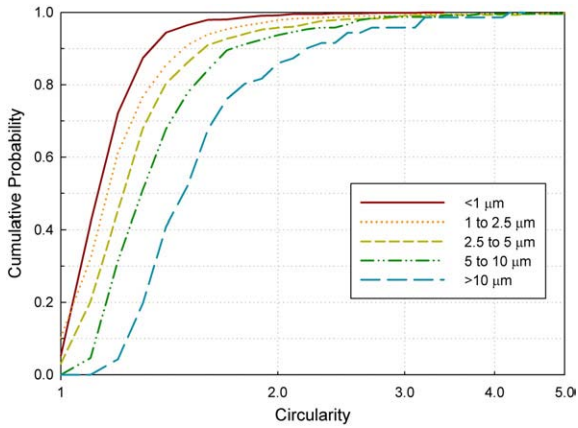


Fig. 5. Cumulative probability plots of shape or circularity for variously sized particles.

were simulated with a daily resolution. Trajectories at the ending time of 00:00, 06:00, 12:00 and 18:00 (UTC) were calculated each day. The sampling altitude was 2700 m above the model ground level. The global reanalysis grid data of 2.5°×2.5° provided by the Climate Diagnostics Center NCEP/NCAR I (CDC-I) Meteorological Data (reproduced by the Air Resources Laboratory, NOAA) were used to simulate the daily backward trajectories during 2007. The clustering tool inte-

grated in the model was applied to form clusters of trajectories based on the percent change in total space variance (TSV) and calculate the mean backward trajectories of all the clusters.

Three clusters were derived directly from the HYSPLIT model, as shown in Fig. 6. Cluster T\_1 represented transport of air masses originating from the arid regions of Kazakhstan, while T\_3 represented long-range transport by the dominant westerly circulation in the spring and winter. Cluster T\_2 represented the long-range aerosol transport of air masses originated from Siberia. The number of T\_1, T\_2 and T\_3 transport pathways distributed over 12 months is shown in Fig. 6. It can be seen that most of the air masses come from the west, agreeing well with the prevailing westerly. Although the air masses originated from three different sources, they all passed through the arid and semi-arid regions of central Asia, which may contribute to the abundant mineral particles. Previous research has shown that synoptic processes favorable in the Tianshan occurred from the west, suggesting that aerosol particles from western Kyrgyzstan, Kazakhstan, Uzbekistan and Turkmenistan may be transported to the east (Aizen et al., 2004). Higher numbers of T\_1 during September and October were consistent with dust storms from western central Asia. It can also be seen that the dominant transport pathways over this region did not pass over the urban area of Ürümqi, which is located northeast of the sampling site. This result further suggests that transport of pollution from Ürümqi to the site was not significant.

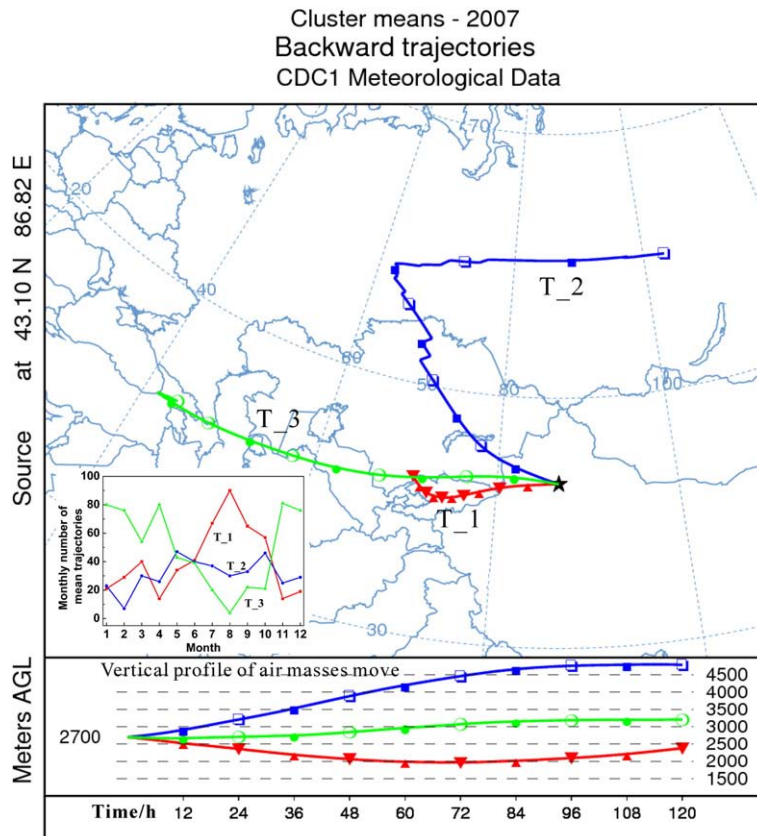


Fig. 6. Cluster means trajectories ending at the sampling site of the Ürümqi Glacier No. 1 in 2007.

#### 4. Conclusion

Aerosols collected from Ürümqi Glacier No. 1 during 2007 were characterized by SEM-EDX to obtain information regarding the size, elemental composition and morphological properties of individual particles. Most of the particles were irregular mineral particles (such as aluminosilicates, quartz, and calcite, etc.) with the sizes smaller than 2.5  $\mu\text{m}$ . Only 1.7% of the particles (little Fe-rich particles and S-rich particles) were likely emitted by anthropogenic activities, suggesting little impact of anthropogenic pollution during the study. Seasonal variations of size, circularity distributions and number concentrations were likely attributed to the different meteorological factors. The frequency of dust storms appears to be the main factor affecting aerosols in spring and autumn, while precipitation during summer and a strong inversion layer in winter may have decreased aerosols. Investigation of air mass back-trajectories indicated that air masses terminating at the sampling site all passed through the arid and semi-arid regions of central Asia, the likely source of dust to the site.

#### Acknowledgements

We appreciate helpful comments from the anonymous reviewers. This research was supported by 973 Project (2007CB411501), the National Natural Science Foundation of China (40631001, 40701034, and 40701035), and the Knowledge Innovation Project of the Chinese Academy of Sciences (KZCX2-YW-127). Support for this research has been provided under the Program for Glacier Processes Investigation (PGPI) conducted by the Tianshan Glaciological Station (TGS), Chinese Academy of Sciences (CAS).

#### References

- Aizen, V.B., Aizen, E.M., Melack, J.M., Kreutz, K.J., Cecil, L.D., 2004. Association between atmospheric circulation patterns and firn-ice core records from the Inilchek glacierized area, central Tien Shan, Asia. *Journal of Geophysical Research* 109, D08304 doi:10.1029/2003JD003894.
- Arimoto, R., Kim, Y.J., Kim, Y.P., Quinn, P.K., Bates, T.S., Anderson, T.L., Gong, S., Uno, I., Chin, M., Huebert, B.J., Clarke, A.D., Shinozuka, Y., Weber, R.J., Anderson, J.R., Guazzotti, S.A., Sullivan, R.C., Sodeman, D.A., Prather, K.A., Sokolik, I.N., 2006. Characterization of Asian Dust during ACE-Asia. *Global and Planetary Change* 52, 23–56.
- Bernabe, J.M., Carretero, M.I., Galan, E., 2005. Mineralogy and origin of atmospheric particles in the industrial area of Huelva (SW Spain). *Atmospheric Environment* 39, 6777–6789.
- Bi, X.H., Feng, Y.C., Wu, J.H., Wang, Y.Q., Zhu, T., 2007. Source apportionment of PM10 in six cities of northern China. *Atmospheric Environment* 41, 903–912.
- Buseck, P.R., Pósfai, M., 1999. Airborne minerals and related aerosol particles: effects on climate and the environment. *Proceedings of National Academy of Sciences of the United States of America* 96, 3372–3379.
- Claquin, T., Schulz, M., Balkanski, Y.J., 1999. Modeling the mineralogy of atmospheric dust sources. *Journal of Geophysical Research* 104 (D18), 22243–22256.
- Cong, Z., Kang, S., Dong, S., Liu, X., Qin, D., 2010. Elemental and individual particle analysis of atmospheric aerosols from high Himalayas. *Environmental Monitoring and Assessment* 160, 323–335.
- Draxler, R.R., Rolph, G.D., 2003. HYSPLIT (Hybrid Single-Particle Lagrangian Integrated Trajectory) Model access via NOAA ARL READY Website, NOAA Air Resources Laboratory, Silver Spring, MD. <http://www.arl.noaa.gov/ready/hysplit4.html>.
- Duan, K.Q., Thompson, L.G., Yao, T., Davis, M.E., Mosley-Thompson, E., 2007. A 1000 year history of atmospheric sulfate concentrations in southern Asia as recorded by a Himalayan ice core. *Geophysical Research Letters* 34 (1) doi:10.1029/2006GL027456.
- Gao, Y., Anderson, J., Hua, X., 2007. Dust characteristics over the North Pacific observed through shipboard measurements during the ACE-Asia experiment. *Atmospheric Environment* 41, 7907–7922.
- Hoonnaert, S., Godoi, R.H.M., Grieken, R.V., 2004. Elemental and single particle aerosol characterisation at a background station in Kazakhstan. *Journal of Atmospheric Chemistry* 48, 301–315.
- Hu, T., Lee, S., Cao, J., Chow, J.C., Watson, J.G., Ho, K., Ho, W., Rong, B., An, Z., 2009. Characterization of winter airborne particles at Emperor Qin's Terra-cotta Museum, China. *Science of the Total Environment* 407, 5319–5327.
- Leck, C., Bigg, E.K., 2008. Comparison of sources and nature of the tropical aerosol with the summer high Arctic aerosol. *Tellus* 60B, 118–126.
- Li, J., Pósfai, M., Hobbs, P.V., Buseck, P.R., 2003a. Individual aerosol particles from biomass burning in southern Africa: 2, compositions and aging of inorganic particles. *Journal of Geophysical Research* 108 (D13,8484) doi:10.1029/2002JD002310.
- Li, Z., Han, T., Jing, Z., Yang, H., Jiao, K., 2003b. A summary of 40-years observed variation facts of climate and Glacier No. 1 at headwater of Ürümqi River, Tianshan, China. (in Chinese). *Journal of Glaciology and Geocryology* 25 (2), 117–123.
- Li, J., Zhang, G., Li, X., Yu, S., Wu, Y., 2005. Analysis of seasonal variation of PM10 concentration and morphology: taking Tianshan District, Ürumqi in 2004 as example (in Chinese). *Urban Environment & Urban Ecology* 18 (6), 16–18.
- Li, Z., Edwards, R., Mosley-Thompson, E., Wang, F., 2006. Seasonal variabilities of ionic concentrations in surface snow and elution process in snow-firn packs at PGPI site on Glacier No. 1, in eastern Tianshan, China. *Annals of Glaciology* 43, 250–256.
- Li, Z., Li, C., Li, Y., Wang, F., 2007. Preliminary results from measurements of selected trace metals in the snow-firn pack on Ürümqi glacier No. 1, eastern Tien Shan, China. *Journal of Glaciology* 53 (182), 1–7.
- Liu, B.Y.H., Pui, D.Y.H., Rubow, K.L., 1984. Characteristics of air sampling filter media. In: Marple, V.A., Liu, B.Y.H. (Eds.), *Aerosols in the mining and industrial work environments*. Vol. 3: Instrumentation. Butterworth-Heinemann, Newton, Mass, pp. 989–1038.
- Luo, H.Z., 1983. Hydrochemical features of the No. 1 Glacier in the source region of Ürümqi River, Tianshan. *Journal of Glaciology and Geocryology* 5 (2), 55–64.
- Marenco, F., Bonasoni, P., Calzolari, F., Ceriani, M., Chiari, M., Cristofanelli, P., D'Alessandro, A., Fermo, P., Lucarelli, F., Mazzei, F., Nava, S., Piazzalunga, A., Prati, P., Valli, G., Vecchi, R., 2006. Characterization of atmospheric aerosols at Monte Cimone, Italy, during summer 2004: source apportionment and transport mechanisms. *Journal of Geophysical Research* 111 (D24202) doi:10.1029/2006JD007145.
- Ming, J., Zhang, D., Kang, S., et al., 2007. Aerosol and fresh snow chemistry in the East Rongbuk Glacier on the northern slope of Mt. Qomolangma (Everest). *Journal of Geophysical Research* 112 (D15307) doi:10.1029/2007JD008618.
- Ming, J., Cachier, H., Xiao, C., Qin, D., Kang, S., Hou, S., Xu, J., 2008. Black carbon record based on a shallow Himalayan ice core and its climatic implications. *Atmospheric Chemistry and Physics* 8, 1343–1352.
- Okada, K., Kai, K.J., 2004. Atmospheric mineral particles collected at Qira in the Taklamakan Desert, China. *Atmospheric Environment* 38, 6927–6935.
- Okada, K., Heintzenberg, J., Kai, K., Qin, Y., 2001. Shape of atmospheric mineral particles collected in three Chinese arid-regions. *Geophysical Research Letters* 28 (16), 3123–3126.
- Orlovsky, L., Orlovsky, N., Durdyev, A., 2005. Dust storms in Turkmenistan. *Journal of Arid Environment* 60, 83–97.
- Paoletti, L., De Berardis, B., Diociaiuti, M., 2002. Physico-chemical characterisation of the inhalable particulate matter (PM10) in an urban area: an analysis of the seasonal trend. *Science of the Total Environment* 292, 265–275.
- Reid, E.A., Reid, J.S., Meier, M.M., Dunlap, M.R., Cliff, S.S., Broumas, A., Perry, K., Maring, H., 2003. Characterization of African dust transport to Puerto Rico by individual particle and size segregated bulk analysis. *Journal of Geophysical Research* 108 (D19), 8591.
- Semenov, V.K., Smirnov, A., Arefev, V.N., Sinyakov, V.P., Sorokina, L.I., Ignatova, N.I., 2005. Aerosol optical depth over the mountainous region in central Asia (Issyk-Kul Lake, Kyrgyzstan). *Geophysical Research Letters* 32 (L05807) doi:10.1029/2004GL021746.
- Shi, Z.B., Shao, L.Y., Jones, T.P., Whittaker, A.G., Lu, S.L., Bérubé, K.A., He, T.E., Richards, R.J., 2003. Characterization of airborne individual particles collected in an urban area, a satellite city and a clean air area in Beijing, 2001. *Atmospheric Environment* 37, 4097–4108.
- Slezakova, K., Pires, J.C.M., Pereira, M.C., Martins, F.G., Alvim-Ferraz, M.C., 2008. Influence of traffic emissions on the composition of atmospheric particles of different sizes—Part 2: SEM-EDS characterization. *Journal of Atmospheric Chemistry* 60, 221–236.
- Srivastava, A., Jain, V., Srivastava, A., 2009. SEM-EDX analysis of various sizes aerosols in Delhi India. *Environmental Monitoring and Assessment* 150, 405–416.

- Sun, J., Qin, D., Mayewski, P.A., Dibb, J.E., Whitlow, S., Li, Z., Yang, Q., 1998. Soluble species in aerosol and snow and their relationship at Glacier 1, Tien Shan, China. *Journal of Geophysical Research* 103 (D21), 28,021–28,028.
- Takeuchi, N., Li, Z., 2008. Characteristics of surface dust on Ürümqi Glacier No. 1 in the Tien Shan Mountains, China. *Arctic, Antarctic, and Alpine Research* 40 (4), 744–750.
- Wu, G., Yao, T., Xu, B., Tian, L., Li, Z., Duan, K., 2008. Seasonal variations of dust record in the Muztagata ice cores (in Chinese). *Chinese Science Bulletin* 53 (13), 1576–1581.
- Yue, W., Li, X., Liu, J., Li, Y., 2006. Characterization of PM<sub>2.5</sub> in the ambient air of Shanghai city by analyzing individual particle. *Science Total Environment* 368, 916–925.
- Zhang, Y., Kang, E., Liu, C., 1994. Mountain climate analysis in Ürümqi River valley, Tianshan (in Chinese). *Journal of Glaciology and Geocryology* 16, 333–341.
- Zhao, Z., Li, Z., Edwards, R., Wang, F., 2006. Atmosphere-to-snow-to-firn transfer of NO<sub>3</sub><sup>-</sup> on Glacier No. 1, eastern Tien Shan, China. *Annals of Glaciology* 43, 239–244.
- Zhao, Z., Tian, L., Fischer, E., Li, Z., Jiao, K., 2008. Study of chemical composition of precipitation at an alpine site and a rural site in the Ürümqi River valley, Eastern Tien Shan, China. *Atmospheric Environment* 42 (39), 8934–8942.